Chemical Engineering Journal 142 (2008) 331–336

Contents lists available at ScienceDirect

Chemical Engineering Journal

journal homepage: www.elsevier.com/locate/cej

Preparation of large particle MCM-41 and investigation on its fluidization behavior and application in single-walled carbon nanotube production in a fluidized-bed reactor

Xianbin Liu, Hui Sun, Yuan Chen, Raymond Lau, Yanhui Yang*

School of Chemical and Biomedical Engineering, Nanyang Technological University, 62 Nanyang Drive N1.2-B1-18, Singapore 637459, Singapore

ARTICLE INFO

Article history:
Received 21 January 2008
Received in revised form 18 April 2008
Accepted 25 April 2008

Keywords:
MCM-41
Morphology control
Fluidization
SWCNTs

ABSTRACT

Large particle MCM-41 was synthesized using preshaped silica gel as the silica source. The physical properties of MCM-41 samples were characterized by X-ray diffraction (XRD), nitrogen physisorption, and field emission scanning electron microscopy (FESEM). The sample showed highly ordered mesoporous structure and spherical morphology with particle sizes of 20–45 μm by pseudomorphic synthesis. The fluidization study showed that the MCM-41 with large particle size, for the first time, can be well fluidized because of the transformation from Geldart C to Geldart A classification. Furthermore, Co–Mo catalyst using large particle MCM-41 as support was successfully applied for the synthesis of single-walled carbon nanotubes (SWCNTs) in a fluidized-bed reactor. The product was monitored by thermogravimetric analysis (TGA), transmission electron microscopy (TEM), Raman and Fluorescence spectroscopy, which suggested the resulted semiconducting SWCNTs possess the narrow (*n*, *m*) distribution.

1. Introduction

The disclosure of micelle-templated silica (MTS) materials with uniform pore diameters between 2–30 nm, such as MCM-41 (Mobil Composition of Matter) [1] and SBA (Santa Barbara Amorphous) families [2] have attracted considerable attentions in the scientific community. These materials are especially promising as catalysts and catalyst supports because of their large pore volume (>1.0 ml/g), high surface area (>1000 m^2/g), large pore diameter (>2 nm), and narrow pore size distribution. MTS materials offer the opportunity to extend shape-selective catalysis beyond the micropore domains typical of zeolite materials, allowing larger molecules to be handled [3]. By introducing metal ions, MTS shows catalytic activity in synthesizing various nanostructures [4] and hydroconversion of long chain aliphatic [3].

The physicochemical properties of MCM-41 are affected by many factors among which calcination condition plays an important role [5,6]. Being the most common post-treatment to remove the template, calcination affects both physical structure of MTS material and the chemical environment of metal ions supported on it [5]. To assure a uniform bed temperature distribution in the calcinator is extremely important for the metal distribution in the final MCM-41 catalysts. Hot spots in the calcinator will result in the migration of metal ions and the formation of chunky metal oxides particles [6]. Along this line, fluidization of MTS is highly desired.

Fluidization can provide many advantages including continuous handling of particles, excellent gas–solid contact, and high mass and heat transfer efficiency [7,8]. Fluidized-bed reactors have been employed in numerous fields, such as petrochemical industry, biomass gasifiers [9], etc. However, MCM-41, classified as Geldart C [10], is hard to be fluidized due to the low bulk density and small particle size. The fluidization of Geldart C particles commonly involves channeling and agglomeration which greatly decrease the fluidized-bed performance. Therefore, the use of MCM-41 in fluidized-bed reactors for industrial applications is limited.

In the present study, it is reported to synthesize novel MCM-41 particles suitable for fluidization, which will greatly expand the application of MCM-41 in catalytic industries. Large MCM-41 particles with well-reserved spherical morphology are prepared by a pseudomorphic synthesis approach [11]. The physical properties of MCM-41 and its fluidization performance are investigated. Co–Mo catalyst using large particle MCM-41 as catalyst support is also successfully applied for the production of SWCNTs in a fluidized-bed reactor.

* Corresponding author. Tel.: +65 6316 8940; fax: +65 6794 7553.
E-mail address: yhyang@ntu.edu.sg (Y. Yang).

1385-8947/$ – see front matter © 2008 Elsevier B.V. All rights reserved.
doi:10.1016/j.cej.2008.04.035

2. Experimental

2.1. Synthesis

MCM-41 is prepared using cetyltrimethylammonium bromide (CTAB) from Sigma–Aldrich as structure-directing agent; the preshaped silica gel (99.99% SiO_2, particle size: 20–45 μm, product number: S10020C, Silicycle) is the silica source. In a typical synthesis, 1.82 g of CTAB and 0.5 g of NaOH are dissolved in 27 g of H_2O with vigorous stirring at room temperature for 1 h. After adding the preshaped silica gel, the mixture is mechanically stirred for another 45 min before transferring to the autoclave and left at 393 K for 6 h. The solid products are then filtered and dried at 363 K overnight.

2.2. Characterization

Powder X-ray diffraction patterns are recorded with a Bruker AXS D8 diffractometer (under ambient conditions) using filtered Cu Kα radiation. Diffraction data are recorded between 0.5° and 8° (2θ) with a resolution of 0.02° (2θ). Nitrogen adsorption–desorption isotherms are measured at 77 K with a static volumetric instrument Autosorb-3b (Quanta Chrome). Prior to each measurement, the sample is outgassed at 523 K to a residual pressure below 10^{-4} Torr. A Baratron pressure transducer (0.001–10 Torr) is used for low-pressure measurements. The specific surface area is estimated by the Brunauer–Emmett–Teller (BET) equation [12]. The pore size distribution is calculated from the desorption branch using the Barrett–Joyner–Halenda (BJH) method [13]. The FESEM images are obtained with JEOL field emission scanning electron microscope (JSM-6700F-FESEM). Prior to the analysis, the samples are deposited on a sample holder with an adhesive carbon foil and sputtered with gold. Particle size distribution of samples is performed in MASTERSIZER 2000 (Malvern Instruments). The given amount of sample is added to anhydrous ethanol and ultrasonicated for 10 min before analysis. The bulk density of the sample is measured by ULTRAPYCNOMETER 1000 (Quantachrome instruments). TEM images of the SWCNTs contained the catalyst were collected on a JEOL 2010, operated at 200 kV. The solid samples are dispersed in pure ethanol by sonication and 0.05 ml of this suspension is dropped on a copper mesh coated with an amorphous holey carbon film. The ethanol is evaporated prior to the TEM analysis. Thermal gravimetric analysis (TGA) data are collected in on a SDT Q600 thermogravimetric analyzer under air flow of 200 ml/min. The weight change in the sample is monitored over the temperature program from 50 to 1000 °C at 10 °C/min. Raman spectra are collected with a Renishaw in Via Raman system using 633 nm (1.96 eV) laser wavelengths over five random spots on each sample. A laser output of 30 mW is used and the maximum incident power at the sample is approximately 6 mW. Fluorescence spectroscopy measurements are conducted on a Jobin–Yvon Nanolog-3 spectrofluorometer equipped with an IGA (InGaAs) near-infrared (NIR) detector.

2.3. Fluidization

The fluidizing properties of MCM-41 particles are studied in a fluidized-bed reactor 25 mm in diameter and 690 mm in height. A porous plate of 10 μm is used as the gas distributor to allow uniform distribution of gas into the bed. 50 g of the large MCM-41 particles is added to the fluidized bed with an initial static bed height of 205 mm. Compressed air is used as the fluidizing gas and the flow rate is controlled by a metering valve. Pressure drop across the bed is measured by a differential manometer at 75 and 380 mm above the distributor. The height of the solid bed is measured by a ruler attached to the fluidized bed. The schematic of the fluidized-bed setup is shown in Fig. 1.

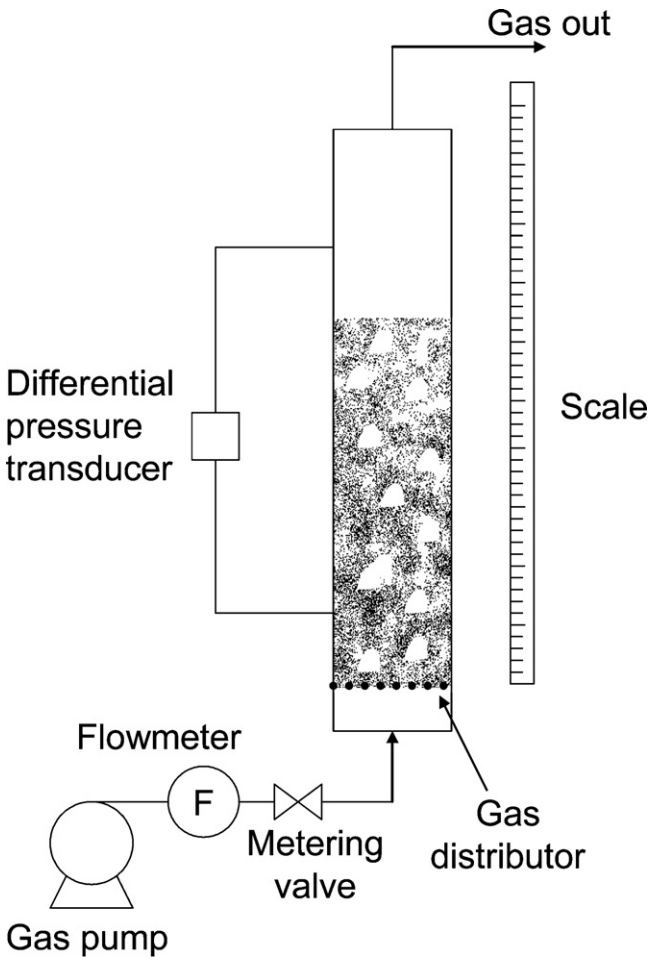

Fig. 1. Schematic diagram for fluidization behavior measurements.

2.4. Preparation of carbon nanotubes

The large particle MCM-41 is applied as a catalyst support. Co–Mo catalysts (total metal loading: ca. 6 wt.%, at a Co/Mo atomic ratio of 1:3) [14–17] are prepared by incipient wetness impregnation of an aqueous solution of cobalt nitrate and ammonium heptamolybdate with MCM-41 particles. The synthesis of SWCNTs is performed in a fluidized-bed reactor. The setup consists of a cylindrical reactor with 1 in. in diameter and 25 in. in height affixed within a high-temperature furnace and control system. The reactor is heated by the electric furnace, equipped with a proportional, integral, and differential temperature controller (Diqi-sense temperature controller *R*/*S*). An extra thermocouple (Type K, Ø0.5 mm) is placed in the interior of the reactor, with the aim of controlling the exact temperature of the catalytic bed. A porous plate of 10 μm is used as the gas distributor to allow uniform distribution of gas into the bed. A filter is place at the outlet of the column to prevent loss of particles. In a typical SWCNTs synthesis, 1.0 g of calcined Co–Mo/MCM-41 catalysts are pre-reduced under 1 bar flowing H_2 (80 sccm) using a temperature ramp 10 K/min to 773 K then hold this temperature for 15–30 min. Subsequently, the reactor is purged using flowing Ar (250 sccm) and the temperature is further increased to 1073 K using a temperature ramp 10 K/min. CO flow of 100 sccm is introduced into the reactor at 6 bar and kept for

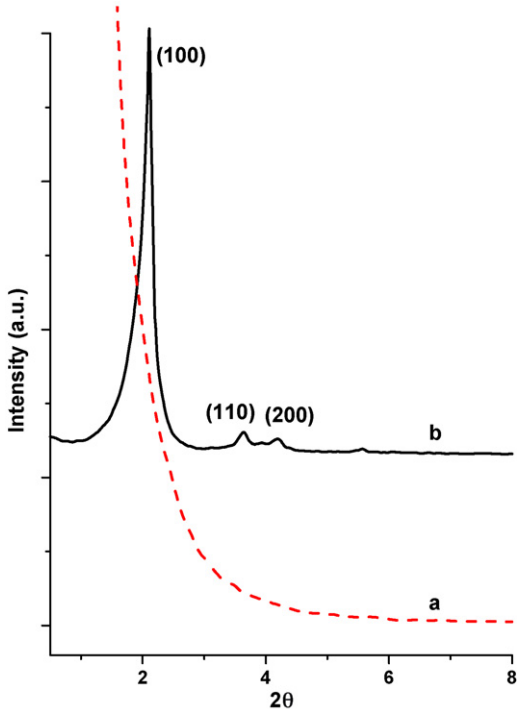

Fig. 2. XRD patterns: (a) preshaped silica gel, (b) MCM-41 prepared from preshaped silica gel.

30 min. The synthesized SWCNTs are refluxed in 1.5 mol/L NaOH solution to dissolve the MCM-41 support and filtered by Nylon membrane with 0.22 μm pore size to remove silica dissolved in NaOH. The purified SWCNTs are suspended in 1% sodium dodecyl benzene sulfonate SDBS/D_2O (99.9 atom% D, Sigma–Aldrich) solution and sonicated using a cup-horn ultrasonication (SONICS, VCX-130) at 20 W for 30 min after ultrasonication, the suspension is centrifuged for 1 h at ca. 53 000 × *g* to remove the catalyst particle and other carbon impurities.

Table 1
Structural parameters for two samples studied

Sample	*d* spacing (nm)	S_{BET} (m^2/g)	Pore size (nm)	V_P (cm^3/g)	Wall thickness (nm)
Preshaped silica	–	480	6.0	0.91	–
MCM-41 from preshaped silica	4.2	828	2.5	0.86	2.3

3. Results and discussion

The pseudomorphic transformations are monitored by X-ray diffraction (shown in Fig. 2). The absence of XRD diffraction peaks in preshaped silica gel sample indicates the lack of long-range order structure. Correspondingly, upon the pseudomorphic transformation, the sample shows one intense (1 0 0) reflection and two well-resolved reflection of (1 1 0) and (2 0 0) peaks at higher 2θ angles. This indicates that the product possesses the long-range order mesoporous structure with hexagonal arrangement [1]. The *d*-spacing calculated from Bragg's equation is 4.2 nm.

Knowledge of the texture and pore structures of solid materials is highly important for the development of catalytic materials. Physisorption is a primary method for characterizing porous materials. The MCM-41 samples have uniform mesopores, ranging from 2 to 10 nm, and have been characterized extensively by nitrogen physisorption. Typical sorption measurements of MCM-41 follow the type IV isotherms, from which the pore structure information including specific surface area and pore size distribution is extracted. The nitrogen physisorption isotherms and pore size distribution results of the preshaped silica and MCM-41 sample obtained from preshaped silica are shown in Fig. 3. The parent silica exhibits type IV adsorption–desorption isotherms with H2 hysteresis loop according to the IUPAC classification; the isotherm presents capillary condensation steps which can originate from the inter-particles pores [19]. The sample shows the presence of broad pore size distribution centered at 6.0 nm and specific surface area of 480 m^2/g. The MCM-41 material by pseudomorphic transformation presents reversible type IV isotherms [20] with a sharp capillary condensation step around $p/p_0 = 0.36$, typical of the structural mesoporosity of MCM-41. A narrow pore size distribution can

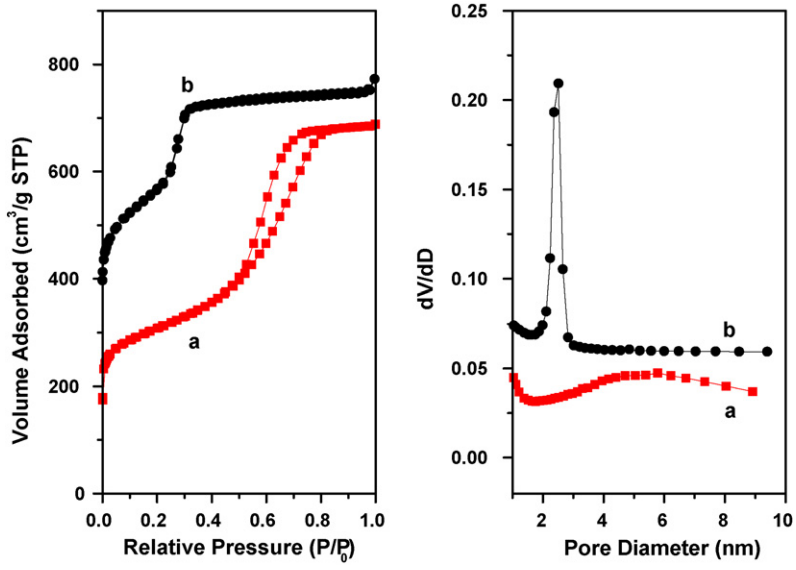

Fig. 3. Nitrogen physisorption isotherms obtained at 77 K (left) and pore size distributions derived from desorption branch by BJH method (right): (a) preshaped silica gel, (b) MCM-41 prepared from preshaped silica gel.

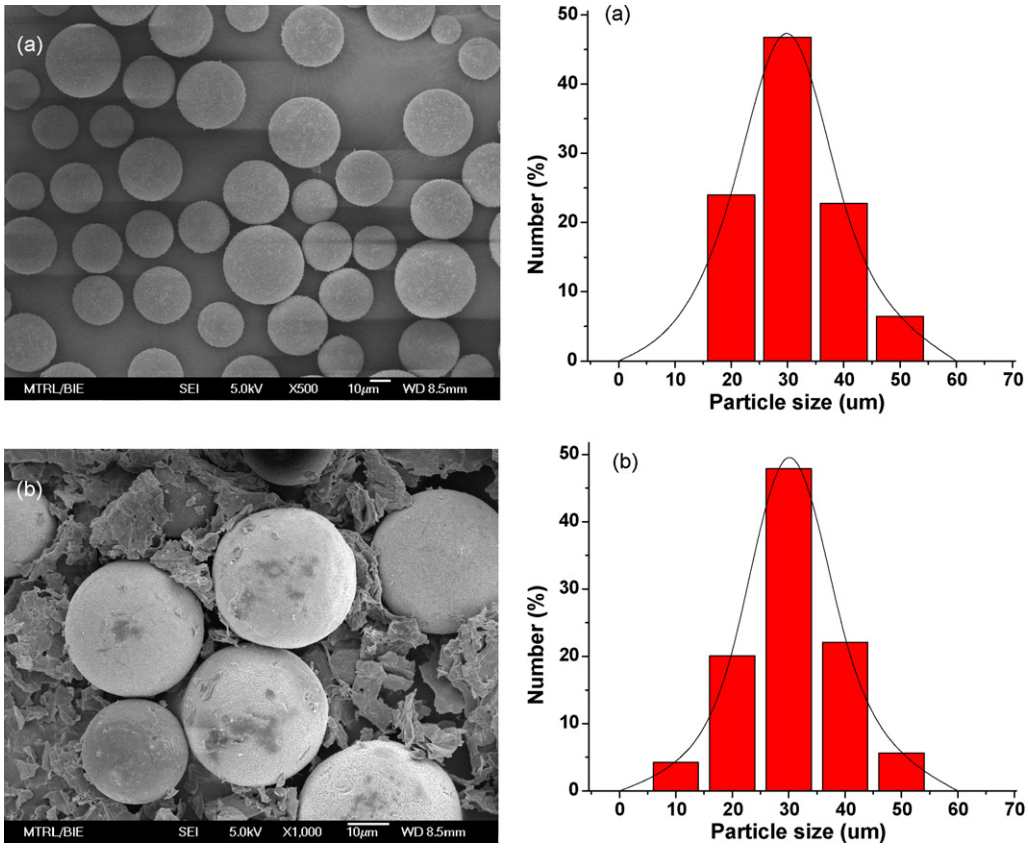

Fig. 4. SEM images and particle size distributions: (a) preshaped silica gel, (b) MCM-41 prepared from preshaped silica gel.

be observed with a mean diameter around 2.5 nm. The sample has a high BET surface area of 828 m^2/g and a pore volume of 0.86 cm^3/g. These results indicate that most of the amorphous parent silica has been successfully transformed to mesoporous MCM-41 upon the pseudomorphic treatment. The adsorption and structural parameters are summarized in Table 1.

Fig. 4 shows FESEM images of the preshaped silica gel and the mesoporous MCM-41 products. The preshaped parent silica gel exhibits a perfectly spherical morphology with diameters range from 20 to 45 μm. After the pseudomorphic transformation, the mesoporous MCM-41 products primarily preserve the spherical morphology. Only a small amount of fragments in products may result from the dissolution silicate. This is due to the minor disbalance between the rates of silicate dissolution and condensation under conditions compatible with the thermodynamics of phase stability [21]. The preshaped silica and the recovered product share the similar spherical morphology and granulometric distribution (in Fig. 4).

Conventional MCM-41 catalysts have a particle size and density range of less than 5 μm and 500–800 kg/m^3, respectively, which fall into the Geldart C particle classification. Geldart C particles are cohesive in nature as the inter-particle contact forces such as van de Waals force, capillary force, and electrostatic forces dominates over the hydrodynamic forces. These particles tend to form agglomerates and thus making the particles difficult to fluidize and gas channeling is commonly observed. The MCM-41 catalysts synthesized by pseudomorphic transformation, however, have particle sizes range between 20 and 45 μm and particle density of 500–1500 kg/m^3. The bulk densities of the sample varied from 500–800 to 500–1500 kg/m^3, because of raw materials come from the different manufacturer and our various post-treatment degrees in synthesis. The increase in particle size moves the particle classification from Geldart C to Geldart A, which is readily fluidizable. Fig. 5 shows the normalized pressure drop result for the calcined large MCM-41 particles measured in a decreasing gas velocity. The minimum fluidization velocity can be determined from the figure to be 18 mm/s. The minimum fluidization velocity is estimated by Wen and Yu's equation [22]:

$$Re_{\mathrm{pmf}} = \sqrt{33.7^2 + 0.0408Ar} - 33.7$$

where $Re_{\mathrm{pmf}} = \rho U_{\mathrm{mf}} d_{\mathrm{p}}/\mu$ and $Ar = \rho(\rho_{\mathrm{p}} - \rho)g d_{\mathrm{p}}^3/\mu^2$. When the average particle size and density are used in the above equations, the minimum fluidization velocity is found to be 0.2 mm/s, which is lower than the experimental value of 18 mm/s. One possibility is

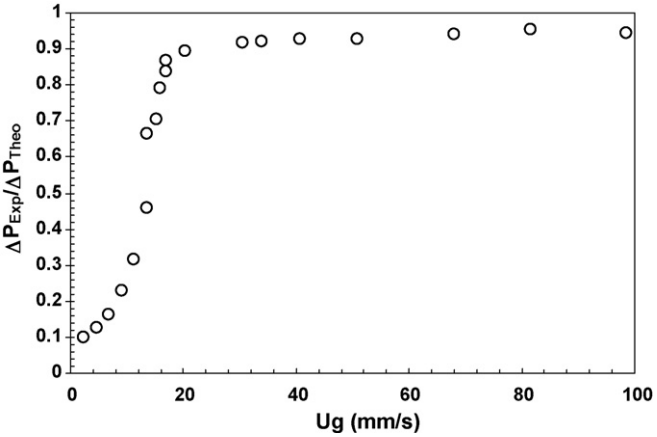

Fig. 5. Normalized pressure drop versus superficial gas velocity for newly calcined large MCM-41 particles.

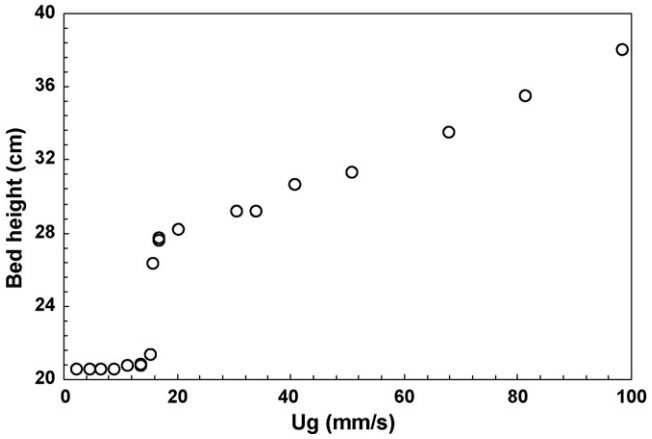

Fig. 6. Bed expansion of calcined MCM-41 large particles.

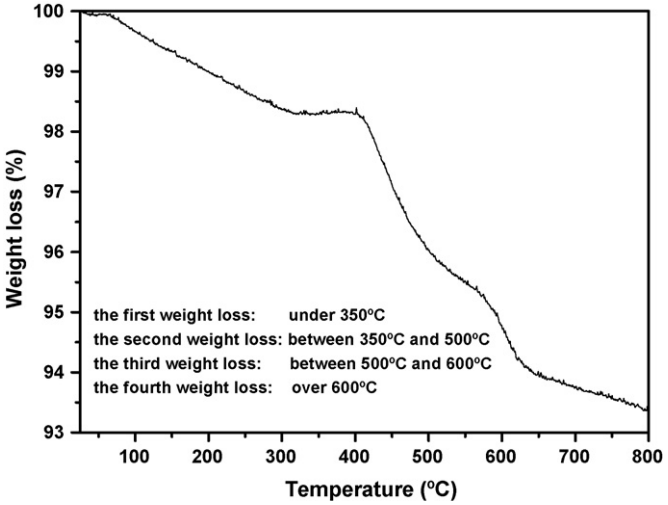

Fig. 7. The TGA curve of SWCNTs contained the catalyst.

that the large MCM-41 particles are fluidized in agglomerate form. Thus, the effective particle size is larger and a higher minimum fluidization velocity is observed. The pressure drop of the large MCM-41 particles remains constant as the gas velocity is increased beyond the minimum fluidization velocity. One possible reason of having the normalized pressure drop of the fully fluidized bed below unity is due to the adhesion of the particles to the column wall during the fluidization process, which reduces the effective weight of the particles.

At the beginning of the experiments, if the gas is introduced abruptly, the top portion of the bed rises as a plug. After the plug rises for a small distance, it starts to disintegrate and fluidize with other particles. However, if the gas is introduced gradually, no plug formation is observed. The large MCM-41 particle is classified as Geldart A particles but the particle size is still relatively small. Therefore, the inter-particle forces still have moderate effect especially during the transition between the packed bed and fluidized-bed regime. The particle bed height is also measured in a decreasing gas velocity and the results are shown in Fig. 6. When the superficial gas velocity is below 16 mm/s, particles are in the packed bed regime and the bed height remains essentially constant. A sharp increase in bed height can be observed between a superficial gas velocity of 16–18 mm/s. This increase in bed height with superficial gas velocity signifies the presence of particulate fluidization regime and is a unique characteristic of Geldart A particles. When the superficial gas velocity is higher than 18 mm/s, owing to the presence of bubbles, a more gradual increase in bed height with superficial gas velocity can be observed. Therefore, the MCM-41 particles synthesized in this study exhibits good fluidization properties and would be suitable for the application in fluidized-bed reactors.

The synthesis of single-walled carbon nanotubes (SWCNTs) is used as a testing experiment in this study to demonstrate the application of MCM-41 as a catalyst support in a fluidized-bed reactor. SWCNTs are grown on Co–Mo catalysts supported on MCM-41 particles using CO as carbon precursor [18,23]. TGA analysis is used to characterize the total carbon loading [17]. The amorphous carbon is completely oxidized at temperatures below 350 °C and graphite burns above 750 °C, the oxidation temperature of the SWCNTs has been observed to vary considerably for samples prepared under different conditions [24,25]. There are four distinct stepwise weight losses in the case of Fig. 7, which can be assigned to amorphous carbon, SWCNTs, carbon nanoparticle successively from low temperature, according to the literature [24,26]. The weight loss between 350 and 500 °C is due to SWCNTs, whereas that over 500 °C is due to multiwalled nanotubes, nanofibers, and graphitic carbon in our study. The representative images of SWCNTs are shown in Fig. 8. Note that the SWCNTs synthesized in our study (in Fig. 8(left)) are in a close-packed hexagonal arrangement, characteristic of tubular structures having uniform diameter [4]. Furthermore, the tube in diameter is ca 2 nm in Fig. 8(right). Raman

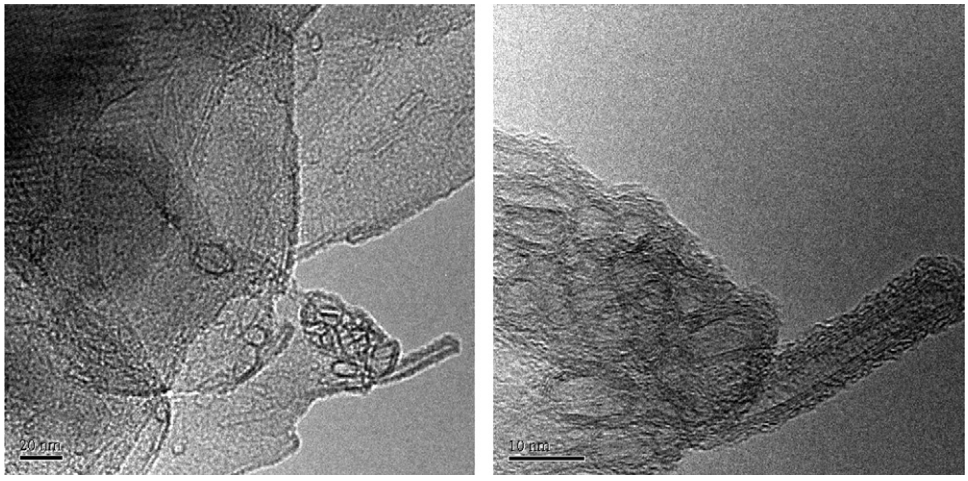

Fig. 8. The TEM images of the sample (left) at low resolution, and (right) at higher resolution.

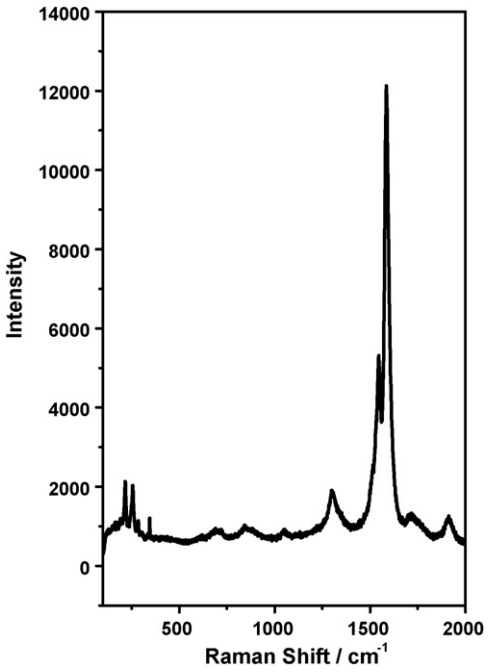

Fig. 9. Raman spectrum of SWCNTs produced from CO disproportionation over Co–Mo catalyst supported on large particle MCM-41.

spectroscopy is a powerful technique for the characterization of the structure of carbon nanotubes. Fig. 9 shows Raman spectrum for carbon deposits excited by 633 nm laser. The typical spectral features of SWCNTs include the radial breathing mode (RBM) below 300 cm^{-1}, the D band around 1300–1350 cm^{-1} and the G band around 1550–1650 cm^{-1}. The intense RBM peaks at 256 cm^{-1} suggest that SWCNTs have been successfully produced in this work under the fluidization condition of MCM-41 [4]. Observation of several peaks in the RBM region (at 256 cm^{-1}) for the SWCNTs grown with the catalyst is direct evidence that the Raman spectroscopy using the 633 nm laser line is sensitive to the broadening of the diameter distribution of the SWCNTs in our samples, and can be used as a relative measure of diameter uniformity. Fig. 10 illustrates the two-dimensional PL excitation map for the aqueous dispersion of SWCNTs with excitation scanned from 300 to 800 nm and emission collected from 830 to 1360 nm. The resonance behavior of both excitation and emission events results in spikes corresponding to the transition pair from individual semiconducting (n, m) SWCNTs [24]. It suggests resulted semiconducting SWCNTs possess the narrow (n, m) distribution.

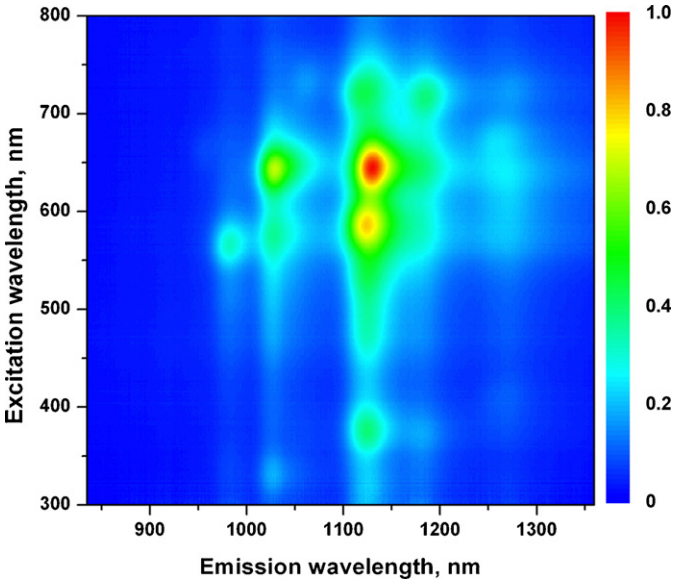

Fig. 10. Photoluminescence excitation (PLE) intensity map as a function of excitation and emission wavelength for SDBS micellarized SWCNTs in D_2O produced from CO disproportionation over Co–Mo catalyst supported on large particle MCM-41.

4. Conclusions

The large particle MCM-41 is successfully prepared, and it possesses ordered mesostructure and spherical morphology as evidenced by XRD and FESEM. The particle sizes of MCM-41 stay within 20–45 μm. The fluidization study shows that the large particle MCM-41 can be readily fluidized in the form of agglomerates and the exhibits both particulate and bubbling fluidization. The catalytic production of SWCNTs in a fluidized-bed reactor is also demonstrated using this large particle MCM-41 as support. It is evidenced that the MCM-41 particles synthesized in this study will be promising for the application in fluidized-bed reactors. The results will broaden the application of MCM-41 as a heterogeneous catalyst in chemical reactions.

Acknowledgment

We are grateful to the Start-up Grant of College of Engineering, Nanyang Technological University, Singapore, for financial support. We also thank to AcRF tier 1 Grant RG45/06 and AcRF Grant RG 118/06 for partial financial support. The financial support of A*STAR project 062 101 0035 is gratefully acknowledged.

References

[1] J.S. Beck, J.C. Vartuli, W.J. Roth, M.E. Leonowicz, C.T. Kresge, K.D. Schmidt, C.T.W. Chu, D.H. Olson, E.W. Sheppard, S.B. McCullen, J.B. Higgins, J.L. Schlenker, J. Am. Chem. Soc. 114 (1992) 10834.
[2] D.Y. Zhao, J.L. Feng, Q.S. Huo, N. Melosh, G.H. Fredrickson, B.F. Chmelka, G.D. Stucky, Science 279 (1998) 548.
[3] A. Corma, Chem. Rev. 97 (1997) 2373.
[4] Y. Chen, D. Ciuparu, S. Lim, Y. Yang, G.L. Harrer, L. Pfefferle, J. Catal. 225 (2004) 453.
[5] F. Kleitz, W. Schmidt, F. Schüth, Micropor. Mesopor. Mater. 65 (2003) 1.
[6] S. Lim, Y. Yang, D. Ciuparu, C. Wang, Y. Chen, L. Pfefferle, G.L. Harrer, Top. Catal. 34 (2005) 31.
[7] J. Jung, D. Gidaspow, J. Nanoparticle Res. 4 (2003) 483.
[8] C.H. See, A.T. Harris, Ind. Eng. Chem. Res. 46 (2007) 997.
[9] T. Nordgreen, T. Liliedahl, K. Sjostrom, Fuel 85 (2006) 689.
[10] D. Geldart, Powder Tech. 7 (1973) 285.
[11] T. Martin, A. Galarneau, F.Di. Renzo, F. Fajula, D. Plee, Angew. Chem. Int. Ed. 41 (2002) 2590.
[12] S. Brunauer, P.H. Emmet, E. Teller, J. Am. Chem. Soc. 60 (1938) 309.
[13] E.P. Barret, L.G. Joyner, P.P. Halenda, J. Am. Chem. Soc. 73 (1951) 373.
[14] D.E. Resasco, B. Kitiyanan, J.H. Harwell, W. Alvarez, US Patent 6,333,016 B1 (2001).
[15] D.E. Resasco, B. Kitiyanan, W. Alvarez, L. Balzano, US Patent 6,413,487 B1 (2002).
[16] D.E. Resasco, B. Kitiyanan, J.H. Harwell, W. Alvarez, US Patent 6,962,892 B2 (2005).
[17] W.E. Alvarez, F. Pompeo, J.E. Herrera, L. Balzano, D.E. Resasco, Chem. Mater. 14 (2002) 1853.
[18] B. Wang, C.H. Patrick Poa, L. Wei, L.-J. Li, Y. Yang, Y. Chen, J. Am. Chem. Soc. 129 (2007) 9014.
[19] M. Kruk, M. Jaroniec, Chem. Mater. 13 (2001) 3169.
[20] P.J. Branton, P.G. Hall, K.S.W. Sing, J. Chem. Soc., Faraday Trans. 90 (1994) 2965.
[21] B. Lefèvre, A. Galarneau, J. Iapichella, C. Petitto, F.Di. Renzo, F. Fajula, Z. Bayram-Hahn, R. Sckudas, K. Unger, Chem. Mater. 17 (2005) 601.
[22] C.Y. Wen, Y.H. Yu, Chem. Eng. Prog. Symp. Ser. 62 (1966) 100.
[23] S.M. Bachilo, L. Balzano, J.E. Herrera, F. Pompeo, D.E. Resasco, R.B. Weisman, J. Am. Chem. Soc. 125 (2003) 11186.
[24] S.M. Bachilo, M.S. Strano, C. Kittrell, R.H. Hauge, R.E. Smalley, R.B. Weisman, Science 298 (2002) 2361.
[25] Z. Shi, Y. Lian, F. Liao, X. Zhou, Z. Gua, Y. Zhang, S. Iijima, Solid State Commun. 112 (1999) 35.
[26] L.S.K. Pang, J.D. Saxby, S.P. Chatfield, J. Phys. Chem. 97 (1993) 6941.